ADVANCED MATERIALS TECHNOLOGIES
www.advmattechnol.de

Chlorophylls as Molecular Semiconductors: Introduction and State of Art

Gabriella Buscemi, Danilo Vona, Massimo Trotta, Francesco Milano, and Gianluca M. Farinola**

Chlorophylls (Chls) and their derivatives are the most common pigments used for light absorption, energy transfer, and charge separation in photosynthetic organisms. Their functions change upon different aggregation states and specific pigment–protein interactions. Differences in the aromatic π-system and substituents finely tune Chls electronic, spectroscopic, and supramolecular characteristics. The varieties of Chls species and the possibility of chemical manipulation, together with their exceptional absorption cross section, make them attractive materials for applications as sensitizer in energy conversion devices. Moreover, when deposited as thin films, Chls and their semi-synthetic derivatives exhibit the typical behavior of molecular organic semiconductors with good charge carrier mobility and Fermi level suitable for their use in optoelectronic devices like phototransistors. This review aims at bridging the possible knowledge and language gap between biochemists and biophysicists working on Chls, and material scientists developing organic optoelectronic devices. Starting from the structural features, and proceeding towards optoelectronic devices, the review offers a critical overview on the uses of Chls as light-responsive molecular semiconductors known so far. Exploiting the high efficiency of these renewable, biocompatible, and recyclable natural systems can pave the way for next generation biooptoelectronics, including artificial light energy converters, photodetectors, and, more in general, forward-thinking technologies.

1. Introduction

The generic name Chlorophyll (Chl) indicates a group of cyclic tetrapyrroles constituting the most abundant pigments present in nature, even visible from the outer space. Such pigments play a pivotal role in the photosynthesis, the metabolic process that fuels the entire biosphere by converting the energy associated to the solar radiation into chemical energy through the fixation of CO_2 into carbohydrates.[1] Chlorophylls are involved in the three major reactions of the photosynthetic process, namely i) absorption of the light radiation acting as antennas in the light harvesting complexes, ii) transfer of the excitation energy to the so-called reaction center proteins, iii) accomplishment of the photoinduced primary charge separation across the photosynthetic membrane. Photosynthetic organisms are found among Eukarya and Bacteria, with large differences in their photosynthetic apparatus (**Figure 1**).[2]

Plants (superior and inferior) and algae are the two main groups of eukaryotic photosynthetic organisms, both performing oxygenic photosynthesis using water as source of electrons and evolving oxygen, by means of two kinds of reaction centers (RC) named photosystem I (PSI) and II (PSII) acting in sequence in the so-called Z scheme.[1a] Bacteria has the largest variety of photosynthetic organisms that can be grouped into oxygenic organisms, Cyanobacteria, possessing both photosystems, and anoxygenic organisms that do not produce oxygen (pigments biosynthesis is inhibited by its presence) and have only one photosystem.[3] In turn, anoxygenic bacteria can be classified according to the kind of photosystem used: purple bacteria, have PSII-like reaction centers, while green sulfur bacteria have RCs similar to PSI.[4] All these photosystems contain Chls arranged in precise positions within the protein scaffolding and in particular, when arranged as dimers they fulfill the function of primary electron donors. Intact photosynthetic proteins and even whole photosynthetic microorganisms are extensively employed in a large variety of devices as recently reviewed.[5] A non-exhaustive list includes photoelectrochemical cells[6] (possessing also self-healing properties and operating at sub-zero temperatures),[7] dye-sensitized solar cells,[8] transistors,[9] tactile sensors,[10] and photodetectors.[11] Combining the approach of organic

Dr. G. Buscemi, Dr. D. Vona, Prof. G. M. Farinola
Chemistry Department
University of Bari "Aldo Moro"
via Orabona 4, Bari I-70126, Italy
E-mail: gianlucamaria.farinola@uniba.it
Dr. M. Trotta
CNR IPCF
UOS Bari
via Orabona 4, Bari I-70126, Italy
Dr. F. Milano
CNR-ISPA
S. P. Lecce-Monteroni, Lecce I-73100, Italy
E-mail: francesco.milano@cnr.it

The ORCID identification number(s) for the author(s) of this article can be found under https://doi.org/10.1002/admt.202100245.

DOI: 10.1002/admt.202100245

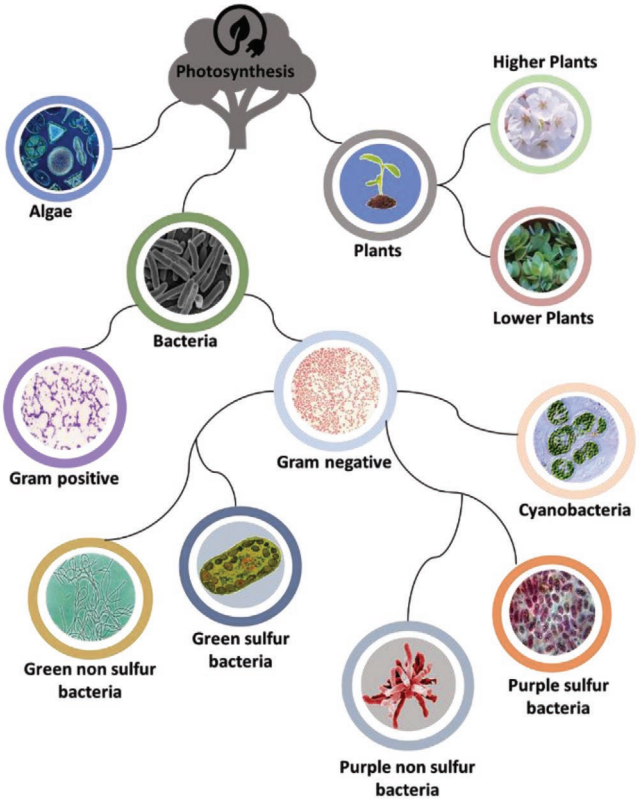

Figure 1. Schematic correlation of photosynthetic microorganisms.

photovoltaics, adopting photosynthetic design principles, and biophotovoltaics, adopting solid-state device architectures, lead to new design concepts based on band-theory.[12]

This large variety of photosynthetic organisms is reflected also in the huge variety of structures of Chlorophylls and Bacteriochlorophylls (BChl), classified on the basis of the degree on unsaturation of the tetrapyrrole ring and its substituents. An important feature of the Chl pigments is their reactivity when arranged in the supramolecular structures of the light harvesting complexes, among which of particular interest are the chlorosomes, large ovoidal envelopes in which a lipid monolayer encloses aggregated pigments, capable of energy transfer over long distances, without any supporting protein matrix.

In this review we will summarize the various kinds of Chls discovered so far and how their structure modulates their spectroscopic features and reactivity. We will then overview the applications of these natural pigments and closely related semisynthetic derivatives, used as organic photoactivated semiconductors or sensitizers. We will show how nature can provide Chls and their derivatives not only as efficient starting materials ready to be integrated in optoelectronic devices but also the guidelines for the construction of artificial antennae and more in general for designing bio-inspired materials for photonic and optoelectronic devices.

2. Chlorophylls and Bacteriochlorophylls Properties

Chls and BChls (from now on collectively termed (B)Chls) are all characterized by a macrocyclic tetrapyrrole scaffold (**Figure 2**) that, due to many structure modifications, can lead to a total amount of nearly 100 Chls known today. Green bacteria possess the largest variety of different structures. The synthesis of the core is common to both eukaryotes and prokaryotes organisms, either photosynthetic or non-photosynthetic. Depending on its oxidation state, the tetrapyrrole ring can be porphyrin, chlorin, or bacteriochlorin. Other differences are in the central metal ligand, functional groups of the macrocycle in C3, C7, C8, C12, C13, and C20, and side chain in C17.[4b] They are all sensitive to oxidation and light, and tend to aggregate interacting with their molecular environments.

2.1. Biosynthesis

The primary building block involved in (B)Chl biosynthesis is 5-aminolevulinic acid (ALA), which begins an enzyme-mediated multistep process (**Figure 3**) involving the sequential production of Porphobilinogen (PGB), Hydroxymethylbilane (HMB), Uroporphyrinogen isomer III (UROGEN), Coproporphyrinogen III (COPROGEN), Protoporphyrinogen IX (PROTOOGEN), and Protoporphyrin IX.

In this pathway, two ALA units are condensed by ALA-dehydratase to form PGB. PGB-deaminase transforms PGB in HMB, a tetrapyrrole linear chain, which is then cyclized and dehydrated by the UPGIII-synthetase, generating UROGEN.[14] Decarboxylation of all acetic side chains to methyl groups leads

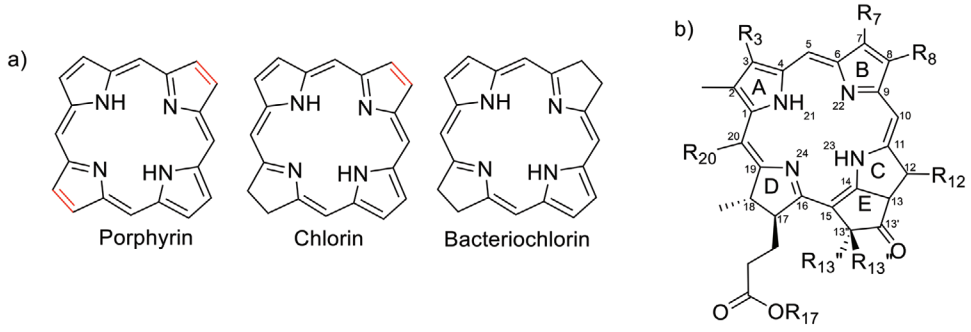

Figure 2. a) Chemical structures of porphyrin, chlorin (17,18-trans-dihydroporphyrin) and bacteriochlorin (7,8-trans,17,18-trans-tetrahydroporphyrin) rings, underlining in red the double bounds progressively reduced. b) IUPAC-IUB numbering of the macrocycle, using chlorin core as representative ring.[13] Numbers 13′ and 13″ are due to the fact that ring E derives from the C-13 propionic acid side-chain of the common heme and Chl precursor, protoporphyrin IX.

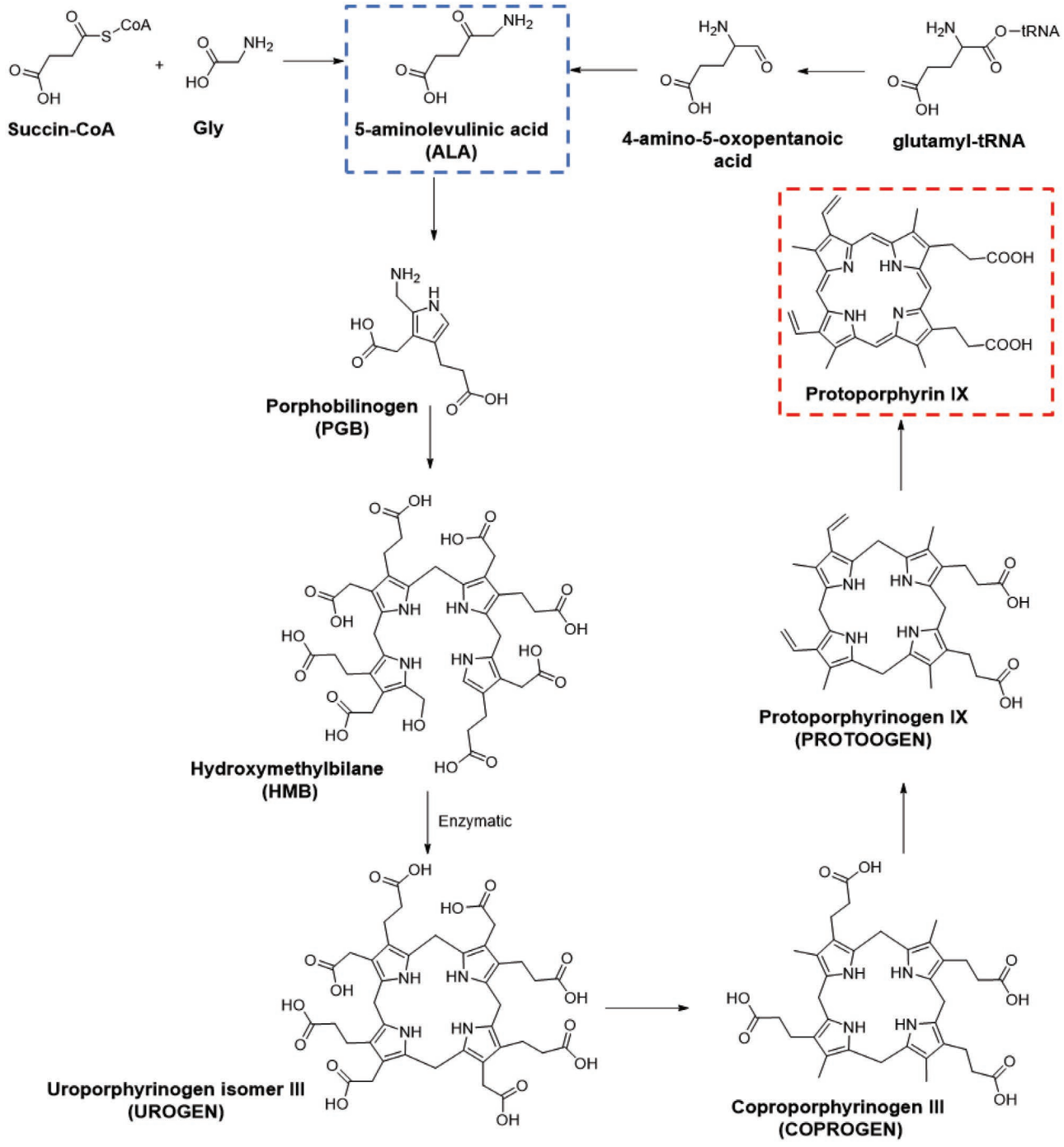

Figure 3. Scheme of the biosynthetic pathway of Mg-protoporphyrin IX.

COPROGEN and subsequent decarboxylation of propionate side chains on two adjacent rings to vinyl groups affords PROTOOGEN. The last step is a six-electron oxidation, mediated by oxygen-dependent and oxygen-independent enzymes, affording protoporphyrin IX as final product.

Protoporphyrin IX is a crucial intermediate in the biosynthesis of tetrapyrrole pigments since it is a precursor of both hemes and (B)Chls. **Figure 4** sketches the biosynthetic pathway leading from protoporphyrin IX to chlorophyllide a.

First, an ATP-assisted magnesium chelation, leads to Mg-protoporphyrin IX, subsequently esterified by methyl transferase. The obtained methylester forms the isocyclic ring E, generating the first chiral center. The obtained vinyl-protochlorophyllide a is reduced in C8, generating protochlorophyllide a. Finally a second reduction on ring D occurs, making two additional

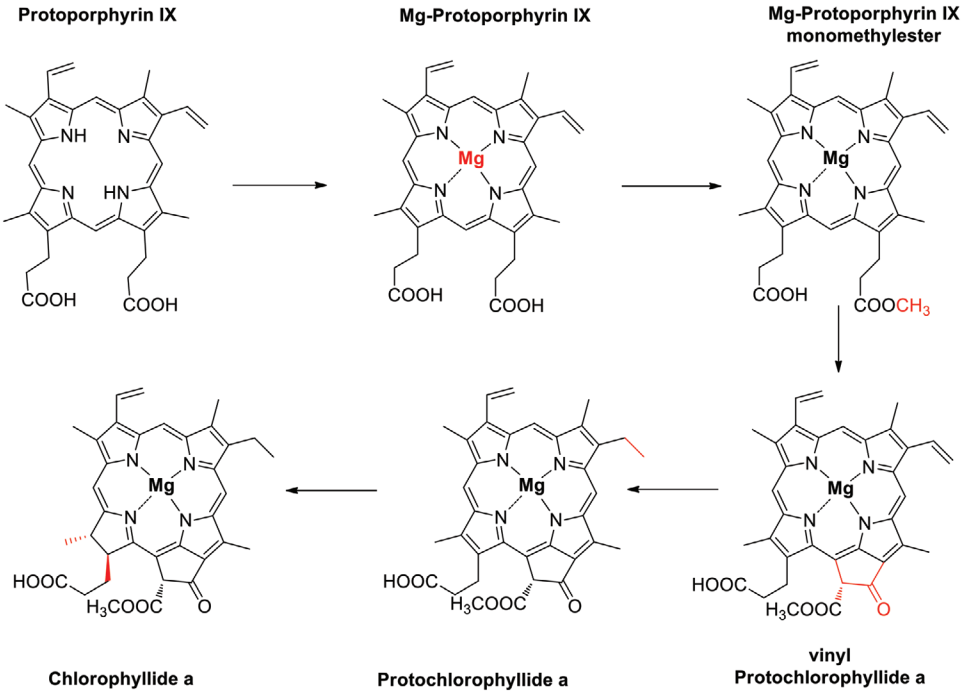

Figure 4. Synthesis of chlorophyllide a from protoporphyrin IX, underlining in red the progressive modifications.

stereo centers (C17 and C18) and generating the chlorophyllide-*a*, that becomes Chl-*a* upon esterification of the carboxylic acid with phytyl diphosphate.[15] Chlorophyllide-*a* is also converted into Chlorophyllide-*b* by enzymatic oxygenase and then to Chl-*b* after the esterification reaction.

2.2. Classification

From a structural point of view, a first classification of (B)Chls can be made on basis of the number of conjugated π-electrons present in the tetrapyrrole scaffold (Figure 2a). In all cases 18 electrons are involved in the aromaticity following the Hückel's rule of $4n+2$ π-electrons, with $n = 4$ for the shortest cyclic path found in bacteriochlorins. However, one and two additional double bonds are involved in the resonant structures of chlorins and porphyrins respectively, hence the total number of conjugated π-electrons are increased to 20 and 22 respectively. (B)Chl cores are planar, but replacement of the inner N—H protons upon chelation with metals can cause some unsteadiness, depending upon the size of the coordinated ion.

As is evident from **Figure 5** and accompanying **Tables 1–3**, the nomenclature of the (B)Chls is not necessarily related to their unsaturation degree or to their origin since BChls include both bacteriochlorins and chlorins, while cyanobacteria and green plants contain the same chlorin type pigments.

The majority of natural (B)Chls contain Mg as the central metal and the C17 propionic acid side chain is esterified with a sesqui- (C_{15}) or di-terpenoid (C_{20}) alcohol. However, there are tetrapyrrolic pigments involved in electron or energy transfer lacking Mg as in the pheophytins or carrying Zn as in some acidophilic purple bacteria.[16] Moreover, most of the c-type Chls lack the esterifying alcohol that, conversely, present large variations in BChls-*c*/*d*/*e* (Figure 5).

2.3. Spectroscopic and Electrochemical Properties

(B)Chls main absorption peaks fall generally in the visible range due to the highly π-conjugated ring structure. The above-mentioned different number of π-electrons and substituents on the tetrapyrrole ring modulates the precise positions and intensity of the absorption peaks leading to different typical colors,[17] as evidenced by the UV–vis–NIR spectra shown in **Figure 6** and **Table 4**.[18]

Solar radiation excites π-electrons of (B)Chls from the ground state S_0 (HOMO and HOMO-1) to two excited states, S_1 (LUMO) and S_2 (LUMO+1), with transitions occurring in about 10^{-15} s. The lower energy required for the $S_0 \rightarrow S_1$ transitions is associated with a red absorptions (600–700 nm) giving rise to the so called Q-bands, while the higher energy required for the $S_0 \rightarrow S_2$ transitions results in blue absorptions (400–500 nm),[3a] giving rise to the Soret or B-bands. In turn, Q bands are distinct by the subscripts x or y depending on whether the starting level involved in the transition is HOMO-1 or HOMO respectively, while the opposite holds for B bands (**Figure 7**). The excited electron in S_2 state quickly loses energy via nonradiative relaxation pathways (molecular vibrations) and decays to the S_1 state by internal conversion in about 10^{-12} s. The electron in the S_1 state, being of lower energy, is stable for a longer time (about 10^{-9} s).[3a]

The fully unsaturated porphyrin macrocycle of the Chl-*c* found in chromophyte algae and in some prokaryotes (Figure 5), presents a major absorption around 450 nm (Soret or B-bands,

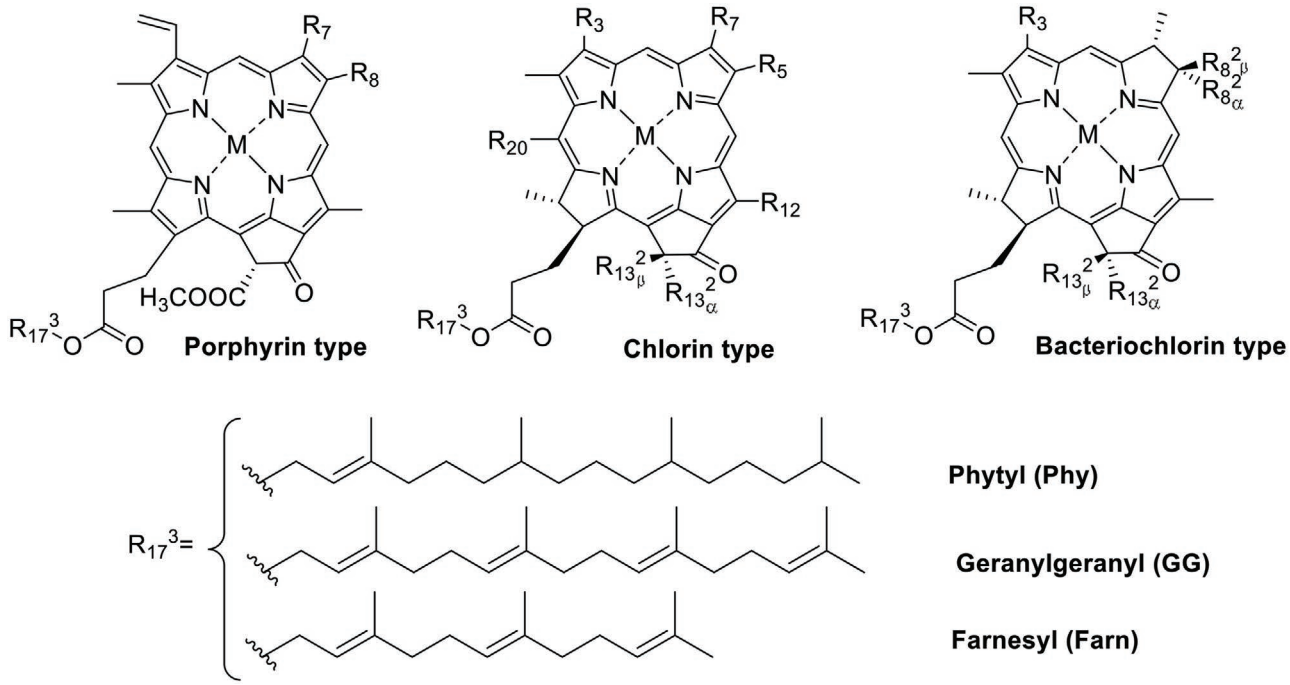

Figure 5. Chemical structures of most common Chls, Bchls, and Porphyrins, and the typical residues R17.

$\varepsilon \approx 150\,000$) and a weak absorption around 620 nm (Q_Y-bands $\varepsilon \approx 20\,000$) as shown by the representative spectrum of Protochl(ide) a in Figure 6. The chlorin system, found in Chl-*a*/*b*/*d* of oxygenic organisms and also in BChls-*c*/*d*/*e* of green anoxygenic bacteria, is characterized by the partial disruption of the conjugated electron shell due to the reduction of the C17-C18 double bond (Figure 2). The lower delocalization degree increases the HOMO energy level and decreases the LUMO one, leading to a smaller energy gap for the S0 → S1 transition. Consequently, in organic solvents these pigments have absorption bands around 440 and 660 nm of equal intensity ($\varepsilon \approx 100\,000$). While all pigments of anoxygenic photosynthetic bacteria are known as BChls, only three of them, BChls-*a*/*b*/*g*, are true bacteriochlorins, characterized by a further lowering of the electrons delocalization degree due to the reduction of the C7-C8 double bond. This leads to a further decrease of the S0 → S1 energy gap and a considerably increased gap among the intense ($\varepsilon \approx 100\,000$) B and Q_Y absorption bands (Figure 6). The Q_Y absorption band is red-shifted to 750–800 nm in monodisperse solution, and even more (800–1020 nm) in vivo,[18] while the Soret-band is blue-shifted (<400 nm) and split. The organisms containing these BChls thereby extend the useable spectrum in both directions beyond those of all other Chls. These pigments also have an appreciably strong absorption band in the visible range (Q_X, $\varepsilon \approx 15\,000$), which has been recognized as a marker band for the state of ligation and H-bonding.[18,20] BChl-*a* is the most widely distributed BChl. It is present in RC and the core-antennas of most anoxygenic bacteria, as well as in the peripheral antennas of the purple bacteria. The presence of different substituents on the tetrapyrrole ring have a great impact on the (B)Chl properties. For instance, Chl-*b* presents in C7, instead of the methyl group found in Chl-*a*, a more nucleophilic formyl group that influences the aggregation properties. Moreover, the electron withdrawing property of the formyl group shifts the maximum absorption to shorter wavelengths. Similar

Table 1. Chlorin-based pigments.

Pigment	R_3	R_7	R_8	R_{12}	$R_{13}{}^2\alpha$	$R_{13}{}^2\beta$	$R_{17}{}^3$	R_{20}	M
Chl-a	C_2H_3	CH_3	C_2H_5	CH_3	$COOCH_3$	H	Phy	H	Mg
Chl-a′	C_2H_3	CH_3	C_2H_5	CH_3	H	$COOCH_3$	Phy	H	Mg
Chl-b	C_2H_3	CHO	C_2H_5	CH_3	$COOCH_3$	H	Phy	H	Mg
Chl-d	CHO	CH_3	C_2H_5	CH_3	$COOCH_3$	H	Phy	H	Mg
Phe-a	C_2H_3	CH_3	C_2H_5	CH_3	$COOCH_3$	H	Phy	H	H_2
BChl-c	$CHOH-CH_3$	CH_3	$CH_2CH_n(CH_3)_{3-n}$	CH_3/C_2H_5	H	$COOCH_3$	Farn/others	CH_3	Mg
BChl-d	$CHOH-CH_3$	CH_3	$CH_2CH_n(CH_3)_{3-n}$	CH_3/C_2H_5	H	$COOCH_3$	Farn/others	H	Mg
BChl-e	$CHOH-CH_3$	CHO	$CH_2CH_n(CH_3)_{3-n}$	CH_3/C_2H_5	H	$COOCH_3$	Farn/others	CH_3	Mg

Table 2. Bacteriochlorin-based pigments.

Pigment	R_3	$R_{8\alpha}/R_{8\beta}$	$R_{13}{}^2\alpha$	$R_{13}{}^2\beta$	$R_{17}{}^3$	M
BChl-a	$COCH_3$	H/C_2H_5	$COCH_3$	H	Phy	Mg
BChl-a′	$COCH_3$	H/C_2H_5	H	$COCH_3$	Phy	Mg
Zn-BChl-a	$COCH_3$	H/C_2H_5	$COCH_3$	H	Phy	Zn
BChl-b	$COCH_3$	$=CH-CH_3$	$COCH_3$	H	Phy	Mg
BChl-g	C_2H_3	$=CH-CH_3$	$COCH_3$	H	GG	Mg
BPhe-a	$COCH_3$	H/C_2H_5	$COCH_3$	H	Phy	H_2
BPhe-b	$COCH_3$	$=CH-CH_3$	$COCH_3$	H	Phy	H_2

variation occurs in Chl-*d*, where the formyl substituent in C3, takes the place of the vinyl group in Chl-*a*.[21]

2.4. Supramolecular Organization of (B)Chls

(B)Chls and carotenoids located in photosynthetic organisms play a key role in their light-driven activities, contributing as light-harvesting complexes (LHCs). In purple bacteria pigments are bounded to two types of low molecular weight hydrophobic apoproteins (α and β), in turn arranged in annular structures through noncovalent interactions. Thanks to the precise spatial arrangement of the bound pigments, the radiant energy is absorbed and transferred to other pigments giving rise to excitation energy transfer (EET), by Förster resonance energy transfer (FRET), or by stronger excitonic quantum coupling, until it arrives to its ultimate acceptor, the RCs. LHCs act also as a self-regulating system, dissipating the excess of incoming radiant energy and allowing the RC to be continuously active for longer time.[22]

A completely different light harvesting architecture is found in green bacteria, containing BChl-*c/d,* whose absorption spectra in solution are very similar to that of Chl-*a*, and BChl-*e/f* carrying a 7-CHO group whose spectra is similar to that of Chl-*b*. This is not surprising since, despite their names, BChl-c/*d*/*e* are chlorins. In vivo, BChl-c/*d*/*e* are present in form of J-type aggregates held together by a combination of hydrogen bonds, coordination bonds, and π–π interactions.[23] The consequent strong excitonic coupling leads to large red shift of their absorption spectra from about 660 nm to 700–750 nm, allowing green bacteria to exploit solar radiation in a broad spectral range down to the near-infrared (NIR) part of the spectrum. The tight packing of these pigments is related to the presence of the $C3^1$—OH group, capable of forming coordinating HO/Mg bond with adjacent pigments, and the absence of the sterically demanding $C13^2$—$COOCH_3$ substituent. Such aggregates (tubular, lamellar, spiral) are found in chlorosomes (**Figure 8**), the extra-membranous peripheral antennae of green bacteria, composed of ovoidal envelope of lipid monolayer and proteins (dimensions of ≈180 nm × 60 nm × 30 nm) containing up to 2×10^5 BChl molecules.[24]

Chlorosomes are therefore structures in which pigment-protein interactions seem to play little or no role, anchored through the so-called baseplate (a region rich in Chl-*a* pigments) and Fenna–Matthews–Olson (FMO) proteins to the photosynthetic membrane in which the RCs are embedded. Upon photon absorption by BChl-*c* aggregates, a series of excitation energy transfer reactions occurs in which each acceptor has longer wavelength maximum absorption with respect to its donor, ultimately funneling the excitation energy to the RCs. The J-aggregates of BChl-*c/d/e* are relatively simple to reproduce in vitro and are used as model systems for artificial light harvesting complexes. Their excellent light-harvesting capability, special light trapping, electron/excited state migration, and hole back-transfer effectively suppressing electron–hole recombination are important features that can be exploited in various kind of optoelectronic devices such as perovskite solar cells,[25] biosolar cells,[26] and for photocatalytic hydrogen evolution reaction.[27] It is important to underline that J-aggregates are formed spontaneously by self-aggregation of BChl-*c/d/e* and related structures (e.g., semisynthetic Zn-Chl) hence the deposition of these structures in ordered manner in the desired device is obtained by simple spin coating.

3. Applications of (B)Chls in Optoelectronic Devices

3.1. (B)Chls as Molecular Organic Semiconductors

Recently, applications of chlorophylls and chlorophyll-enzyme biosensors have been reviewed.[28] Similarly, applications of chlorophylls and porphyrin-based materials in energy conversion have been surveyed in the case of dye-sensitized,[29] and organic[29,30] solar cells. Here, we will hence focus on the application (B)Chls in other kinds of optoelectronic devices, such as

Table 3. Porphyrin-based pigments.

Pigment	R_7	$R_{8\alpha}/R_{8\beta}$	$R_{17}{}^3$	M
Chl(ide)-c_1	CH_3	C_2H_5	H	Mg
Chl(ide)-c_2	CH_3	C_2H_3	H	Mg
Chl(ide)-c_3	$COCH_3$	C_2H_5	H	Mg
ProtoChl(ide)-a	CH_3	C_2H_5	H	Mg

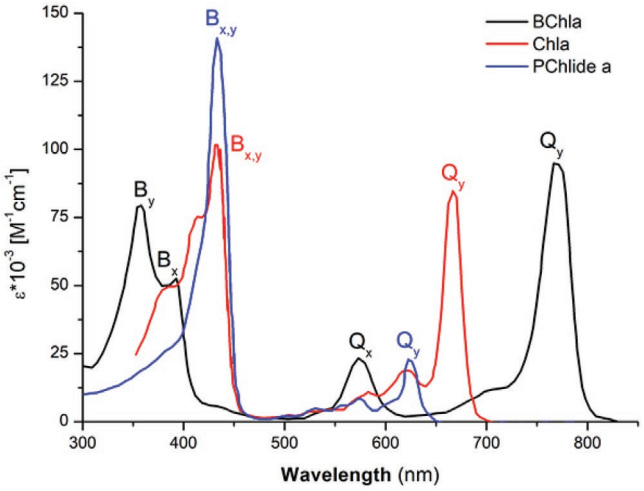

Figure 6. Absorption spectra of (B)Chls underlining the conjugation effects.[19] ProtoChlide a, Chl-*a*, and BChl-*a* are representative of porphyrin, chlorin, and bacteriochlorin-based structures, respectively.

organic phototransistors, in which the semiconducting properties, rather than sensitization, are mainly exploited.

(B)Chls molecules, after deposition as thin films in proper devices configurations, can be in fact viewed as photoactive organic semiconductors (OS). In the case of Chl-*a* a bandgap of 1.9 eV is calculated from its maximum absorption peak at 660 nm, while the HOMO and LUMO levels are −4.9 and −3.2 eV respectively.[31] The suitability of any semiconductor material for applications in electronic devices, such as field effect transistors (FETs), is mainly determined by the charge carrier mobility (μ), defined as the in-plane charge carrier velocity in a solid material under applied electric field (dimensions of cm^2 V^{-1} s^{-1}). Like most of the molecular OS used in optoelectronic devices, (B)Chls films present a disordered structure that, combined with weak van der Waals forces holding together the (B)Chls macrocycles, precludes charge transport in delocalized valence and conduction bands. Instead, charge carriers are preferentially localized at each macrocycle and move by incoherent hopping among adjacent sites with statistically variable energies and distances leading to a density of states (DOS) broadening.[32] Charge carrier mobility results therefore several orders of magnitude lower compared to crystalline systems. However, OS materials present the advantages of low cost and room temperature processing, which is appealing for large area devices, such as flat panel displays based on organic light emitting diodes (OLEDs) technology, potential compatibility with plastic substrates, and chemical tunability allowing fine tuning of properties and performance enhancement based on fine molecular tailoring. The further advantage of using (B)Chls resides in their massive abundance in natural organisms from which can be easily extracted in a variety of different structures, nontoxicity and biodegradability. Charge mobilities in the first OS generation were typically in the range of 10^{-6}–10^{-5} cm^2 V^{-1} s^{-1}, for example for vapor-deposited thin films of polythiophenes,[33] electrophoretically deposited phthalocyanines,[34] and perylene tetracarboxylic acid diimide.[35] In the last years, record values above 40 cm^2 V^{-1} s^{-1} have been reached with OS like rubrene or pentacene in crystalline form,[36] to be compared with values of about 10^3 cm^2 V^{-1} s^{-1} for crystalline inorganic semiconductors (Si, Ge, Ga, As). However, amorphous OS are more reasonably compared with amorphous Si, whose charge mobility is about 1 cm^2 V^{-1} s^{-1}. Values of charge mobility up to 0.28 cm^2 V^{-1} s^{-1} for 2D stacked assemblies of particular Chl derivatives (see later) have been reported.[37] The charge mobility is not an intrinsic property of the material but it depends on the geometry of the experimental setup. For instance, in thin film transistors (TFT) described below, where the current flow is confined in a thin layer, disorder effect on charge carrier motion is diminished, hence the values inferred from these devices are generally higher than those determined from time-of-flight (TOF) experiments.[38] For this reason, in field effect transistors based on organic semiconductors (OFETs), the organic semiconductor is deposited as thin film, and the resulting devices are called also organic thin film transistors (OTFTs).

3.2. Chlorophyll/Metal Junctions

In general, when a semiconductor comes in close contact with a metal, a metal–semiconductor junction (MSJ) is formed, that can be either rectifying or not rectifying. In the latter case the junction is called an ohmic contact, since electrons can freely flow across it in both directions. The rectifying behavior arises when the junction forms the so-called Schottky barrier Φ_B, the potential energy barrier that electrons must overcome to cross it.[39] **Figure 9** depicts a Schottky barrier formed by a metal, characterized by a continuum of electronic states filled up to a common electron chemical potential, often referred to as the

Table 4. Spectroscopic properties of some (B)Chls in vitro.

Pigment	λ_{max} [nm]	ε_{max} [mM^{-1} cm^{-1}]	τ_f [ns]	ϕ_f
Chl-a	662, 578, 430	90.0, 8, 118	6.1	0.35
Chl-b	644, 549, 455	56.2, 7, 175	3.6	0.15
Chl-c (combined)	628, 580, 447	51, 21, 227	6.1	
Chl-d	698, 455	88, 80		
BChl-a	773, 577, 358	91.2, 20.9, 85.4	3	0.2
BChl-b	794, 578, 368	106, 25, 81	2.5	
BChl-c	660, 432	91, 142	6.5	0.29
BChl-d	650, 425	89.9, 115.6	5.6	

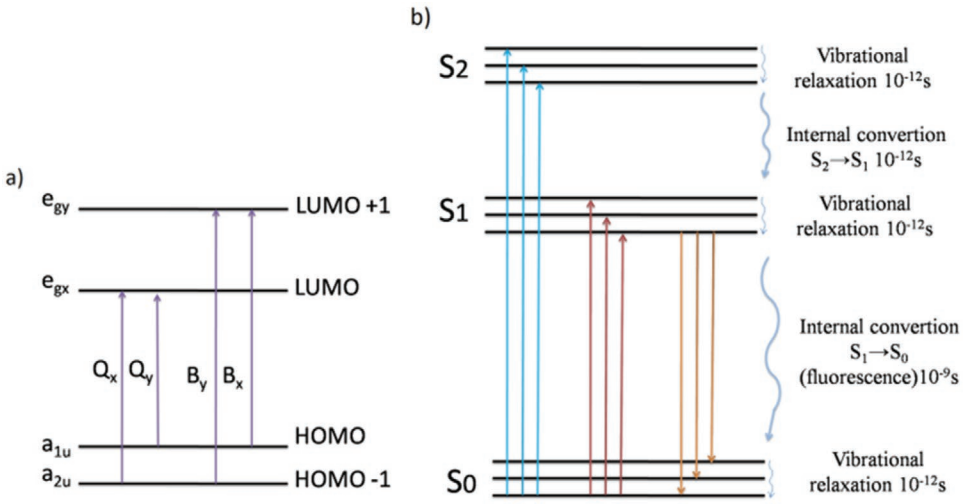

Figure 7. a) Energy levels of the four orbitals involved Q and B bands; b) Jablonski diagram of chlorophylls.

Fermi level (E_F), contacting a n-type inorganic semiconductor in which E_F is closer to the conduction band (for intrinsic semiconductors E_F lies exactly in the middle of the energy gap). In the example, the metal work function Φ_M (i.e., the energy required to bring an electron from E_F to the vacuum level) is higher than the semiconductor work function Φ_S. The Schottky barrier originates from the "band bending" of semiconductor in correspondence of the contact area since the Fermi levels of the two materials tend to equalize. Since $\Phi_M > \Phi_S$, the electrons in the semiconductor have higher energy than in the metal and, upon contacting the two materials, start to flow from the semiconductor to the metal. This results in the formation of a built-in potential E_i and a charge depletion layer over a distance w at the semiconductor side consisting of immobile ionized donors accounting for the rectifying nature of the junction. A vacuum level (E_0) discontinuity across an interface can be observed, commonly attributed to the formation of an electric dipole.

In the case of molecular organic semiconductors like chlorophylls, a similar diagram can be made, substituting the valence and conduction bands with the HOMO and LUMO levels, with the Fermi level in the middle of the energy gap. It was quite early realized that solid layers of Chl behave like photo-semiconductors in which charge carriers are positive charges (holes) (p-type semiconductor) and electrons move at the ground level

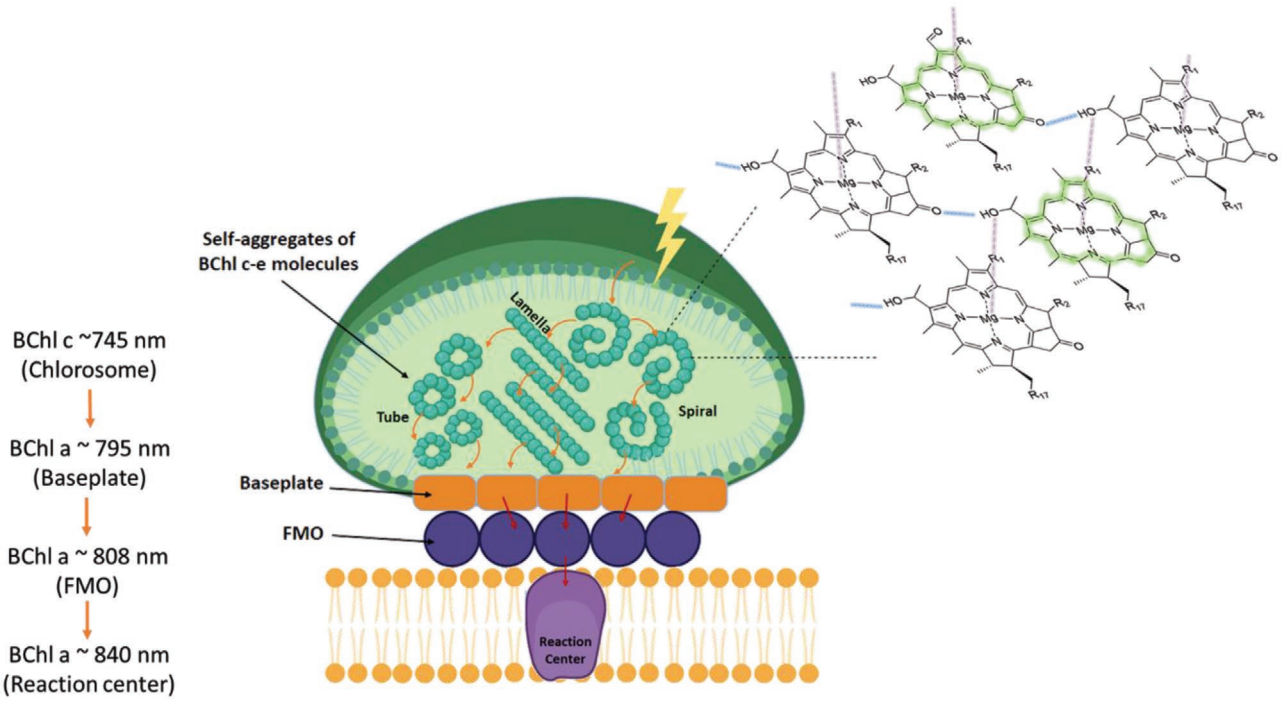

Figure 8. Representation of excitation transfer in chlorosomes and structure of J-aggregates of BChl-c.

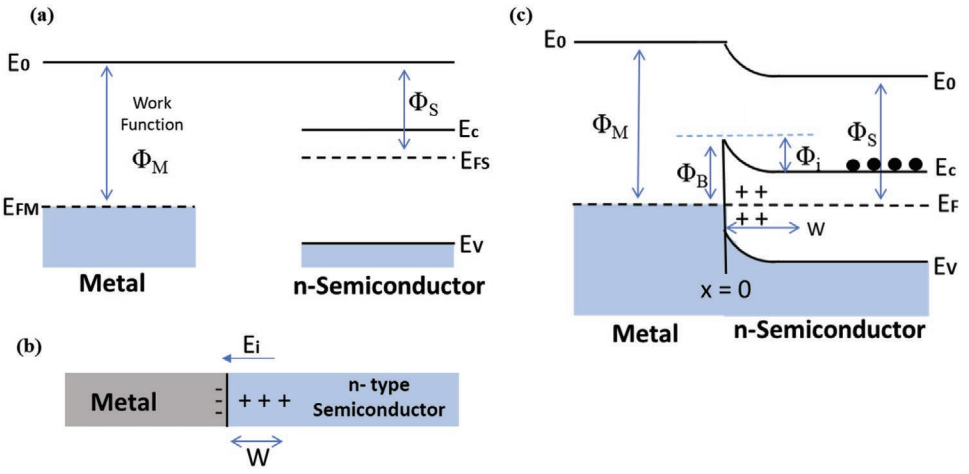

Figure 9. A Schottky barrier formed at the junction between a metal and an n-type semiconductor. a) Metal and semiconductor Fermi energies (E_{FM}, E_{FS}) and work functions (Φ_M, Φ_S), conduction and valence band levels *Ec* and *Ev*, before putting the two materials in contact. b) Electron flow at MSJ forming the charge depletion layer *w*. c) MSJ (junction point at $x = 0$) at equilibrium with a Schottky barrier Φ_B for the flow of electrons (black dots) from the metal to the semiconductor and a barrier Φ_i for the reverse direction. The bent part of the energy bands corresponds to the *w* extension.

in an intermolecular oxidation-reduction exchange process.[40] Moreover, the absorption band of the molecules forming the lattice is only moderately broadened by the close interaction of identical molecules. The contact between the Chl-*a* and a metal is thus relatively more ohmic for metals having a work function higher than the HOMO level of Chl-*a* such as Au (5.1 eV vs 4.93), and more blocking for metals with lower work function such as Al (4.08 eV).[41] This was demonstrated by electrodepositing microcrystalline Chl-*a* film sandwiched between two different metals, obtaining a device showing rather strong photovoltaic effects, that can be seen only in the presence of rectifying behavior at one of the two contact. The active area primarily responsible for the photovoltaic activity is at the junction with the metal having the lower work function. This confirms that a Schottky type barrier is present at this junction and that p-type conduction is implicated in Chl-*a* films.

3.3. Organic Thin Film Transistor Working Principle

An OTFT typically consists of an OS thin film, three metal electrodes (gate, drain and source) and a thin insulating dielectric layer between the OS and the gate electrode. OTFTs are classified as bottom- or top-gate devices depending on whether the gate is placed below or above the semiconductor, and bottom- or top-contact depending on whether the drain and source electrodes are placed below or above the semiconductor. The core of an OTFT (**Figure 10**a) is a metal–insulator–semiconductor structure (MIS), in which the gate (G) and the OS thin film can be considered as the plates of a capacitor separated by a dielectric, typically made of SiO_2. Very commonly the gate is made of heavily doped n^+ Si that acts as a conductor and a few hundred nm thick layer of dielectric SiO_2 is formed on top of it by thermal oxidation of the substrate. In the bottom gate-bottom contacts geometry, the source (S) and drain (D) electrodes are patterned between the dielectric and the OS. If a negative voltage is applied between G and S (V_{GS}), the induced electric field attracts positive charge carriers at the semiconductor/insulator interface between S and D in correspondence of G generating the so-called conducting channel region. The name "field effect" transistor originates exactly from this mechanism. Applying in turn a negative voltage between S and D (V_{DS}), it is possible to drive the positive charge carriers across the channel.

For efficient charge injection into organic semiconductors, the work function of the electrode has to match the highest occupied molecular orbital (HOMO) energy level of p-type

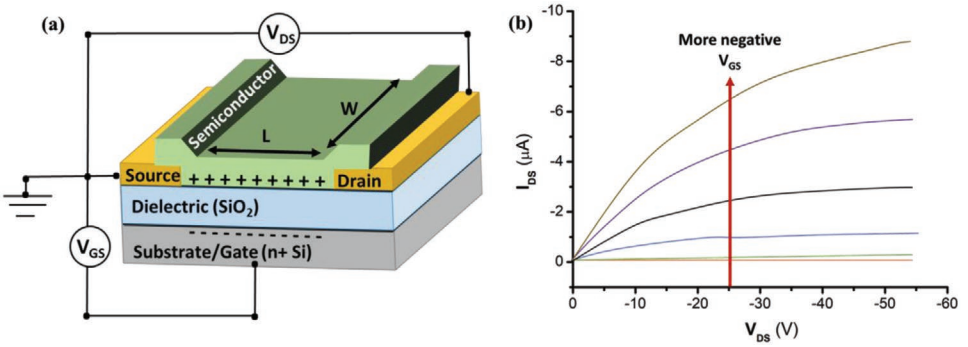

Figure 10. a) Schematic of the OTFTs using the bottom gate—bottom contacts geometry. b) I_{DS}–V_{DS} diagram at increasing V_{GS} values showing the linear and saturation regions.

semiconductors or the lowest unoccupied molecular orbital (LUMO) energy level of n-type semiconductors. In the case of p-type Chl thin film- based OTFT, Au is often the chosen metal. Below a certain threshold voltage V_T, there are not enough free charge carriers in the organic layer and the device is in its off state, that is, minimal current flows between S and D, no matters the amplitude of V_{DS}. When $V_{GS} > V_T$, with a small applied V_{DS}, the electric field induced by G generates a uniform charge distribution along the conducting channel, allowing the device to operate in the linear region. For V_{DS} larger than a certain threshold, a charge carrier depleted area is generated near S and the current flowing across the channel saturates, becoming independent upon further increase of V_{DS}. Obviously, the higher the field effect charge mobility in the OS layer, the larger will be the current flowing between D and S with a fixed combination of V_{GS} and V_{DS}. The field-effect mobility μ can be calculated with the relationship[42]

$$\mu = \frac{L}{W}\frac{1}{V_{DS}C_{ox}}g_m \quad (1)$$

where W, L, and C_{ox} are the channel width, channel length, and the gate capacitance per area respectively and g_m is the transconductance. Typical parameters used to benchmark OTFTs are i) their ability to efficiently switch between on and off states, with a low magnitude V_T, ii) a high on-to-off current ratio (I_{ON}/I_{OFF}), and iii) small response time.

3.4. (B)Chl Based Phototransistors

When it comes to (B)Chl based transistors, besides the intrinsic semiconducting properties of the relevant thin films, their capability of absorb light and generate excited electrons is also exploited. The resulting devices are called photoresponsive organic field-effect transistors (PR-OFETs), in which the current flowing between D and S is not (only) controlled by V_{GS} but (also) by the incident light. In these devices additional performance indicators are introduced: i) the electron/photon gain, defined as the number of electrons flowing between D and S per each incident photon, ii) the ratio between the current intensity obtained under light and in the dark I_{photo}/I_{dark}, iii) the responsivity,[43] defined as the output signal (either voltage or current) produced in response to a given incident radiant power, with unit A/W or V/W, and iv) the specific detectivity D^* (expressed in Jones units, cm × $Hz^{1/2}$ W^{-1}) defined as:

$$D^* = \frac{\sqrt{A\,\Delta f}}{NEP} \quad (2)$$

where NEP is the noise-equivalent power, A is the device's photoactive area, and Δf is the frequency bandwidth. The semiconducting and photosensitive characteristic of (B)Chls are actively exploited in current literature, either as the sole active material or in conjunction with other materials as photosensitizers. This feature has already been used in organic photovoltaics,[44] optical sensors,[45] and other devices.[29]

The most simple architecture of a Chl-based PR-OFET was recently proposed by Yu and coworkers, exhibiting both photoelectric and thermoelectric characteristics.[42] The device consisted of a gate electrode of highly doped n^+ Si covered with a 300 nm thick SiO_2, on top of which the Au source and drain electrodes were thermally evaporated and finally a Chl active layer of 80 nm was deposited via a spin-coating (bottom gate—bottom contact configuration, **Figure 11**a).

In the dark, with $|V_{GS}| > |V_T|$ (ON-state), unipolar transport with standard linear-to-saturation I–V transistor characteristics was observed and explained on the basis of gate-tunable injection barrier at the Au/Chl-*a* interface within a source-to-drain rectifying diode. Rectification in the reverse-bias regime ($V_{DS} > 0$) was observed for $V_{GS} \leq 0$. Since the gold electrode provides an ohmic contact with Chl-*a*,[41] rectification at $V_{GS} = 0$ is mainly due to the electron injection barrier resulting from the energy level mismatch between the Au work function (≈5.1 eV) and the LUMO of Chl-*a* (≈3.18 eV). When negative gate voltage is applied, the work function of the Au increases, creating a larger electron injection barrier and hence higher current rectification is obtained. On the other hand, when the gate is positively biased the work function of the Au decreases, lowering the electron injection barrier height from the source into the organic layer, leading to a larger reverse current (lower rectification).

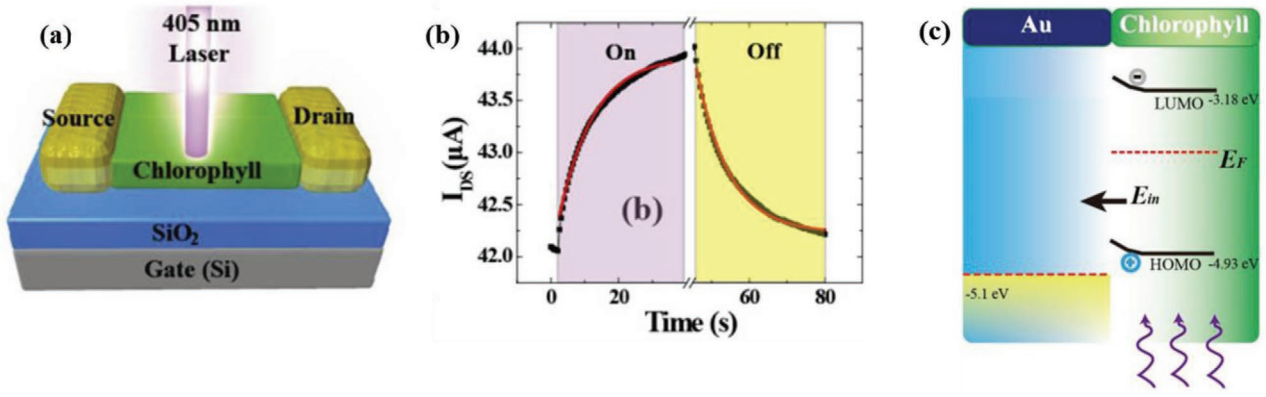

Figure 11. a) Schematic diagram of Chl OFET. b) Temporal photocurrent response of OFET under irradiation. c) Diagram of energy level of the conductor-semiconductor interface upon illumination. Reproduced with permission.[42] Copyright 2018, Elsevier.

The photoresponse was investigated with laser excitation at 405 nm (intensity 1.2 mW cm^{-2}) at V_{GS} = 0.5 V, and V_{DS} = 1 V (Figure 11b). When the light is turned on, the photocurrent increases (time constant τ_{rise} = 20 s) due the photo-induced holes transfer from Chl to Au electrode and subsequent charge transfer in channel (see energy diagram in Figure 11d). When the light is turned off the photocurrent decrease with a time constant τ_{fall} = 30 s representing the lifetime of photo-induced charges in Chl before they transfer to neighboring Au electrode. The long response times may be correlated with the carrier diffusion or trapping in stacks of Chl molecules, which is dominated by the bulk Chl properties, such as mobility and trap density.[46] In the case of the thermoelectric phenomenon, heat induces negligible change of Fermi level in gold, but it significantly increases for Chl, thereby enhancing the hole transfer from Chl to Au similarly, but less efficiently, to the case of light excitation (Figure 11c). Electron and hole mobilities in the Chl thin layer were found to be 2.2×10^{-3} and 5.8×10^{-3} cm^2 V^{-1} s^{-1}, confirming the larger hole mobility. Other key parameters characterizing the device performance were $D^* = 1.4 \times 10^{17}$ Jones, NEP = 3.6×10^{-19} W Hz^{-1}, and $G = 1.5 \times 10^4$. To characterize the Chl/Au Schottky barrier, the authors investigated the *I–V* curves as a function of temperature applying the 3D thermionic emission equation,[47] finding a barrier height Φ_B of 77 meV.

Chen et al.[31] used Chls as sensitizer coupled with graphene in a bio-hybrid phototransistor. Due to its tunable energy band-gap,[48] linear optical absorption,[49] and intrinsic photocurrent,[50] graphene is often integrated in various opto-electronic devices.[51] To overcome its low light absorption (2.3% of incident photons),[49a] the authors developed the graphene-Chl phototransistor shown in **Figure 12**a. A graphene monolayer was mechanically exfoliated onto octadecyltricholorosilanes (OTS) -functionalized SiO_2 substrate followed by laser annealing to remove surface adsorbates (such as H_2O and O_2) to increase charge carrier mobility. Then Chl-*a* was drop-cast with a continuous nitrogen gas flow to functionalize the graphene. Two gold electrodes were deposited on top of this layer, while highly doped n^+ Si served as the gate electrode, placed at the bottom.

The effective electronic interaction between the two materials was demonstrated by measuring the conductance (*G*), proportional to I_{DS}, as a function of V_{GS}. The value of V_{GS} at the charge neutrality point (V_{CNP}), also called Dirac point, shifts from –5 V for pristine graphene to –40 V for graphene/Chl (Figure 12c). This shift reveals that in dark conditions an electron transfer occurs from Chl to graphene (n-type doping), generating a built-in electric field, attributed to the energy level alignment of graphene and Chl, as shown in Figure 12e. Because the Fermi level of Chl (4.1 eV, falling in the middle of the HOMO-LUMO band gap) is higher than that of graphene,[52] the latter is raised when the two materials are brought into contact as electrons transfer from Chl to graphene.[53] Figure 12c shows also the band bending of Chl energy levels, leading to the Schottky barrier. When the light is switched on, the $G–V_{GS}$ curves in Figure 12c show that pristine graphene has no significant photoresponse, but after Chl sensitization the new composite is characterized by an intense and reversible light induced Dirac point shift from –40 to –23 V (Figure 12c). During the illumination, electron-hole couples are generated within the Chl layer due to

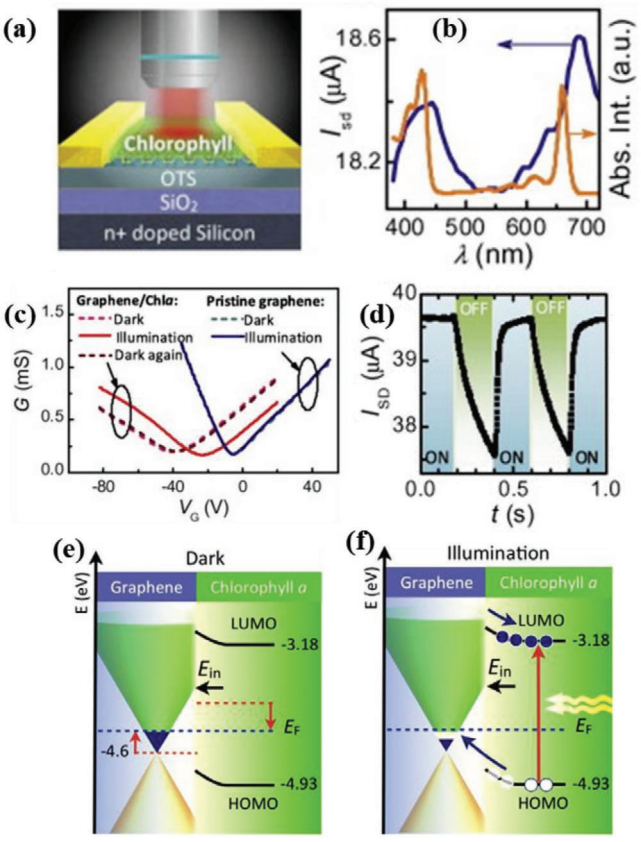

Figure 12. a) Scheme of the graphene-Chla device. b) Photocurrent action spectrum of graphene-Chla (blue line) overlap with the absorption spectrum of Chla (orange line). c) G–VG curves of pristine graphene and graphene-Chla with and without illumination (683 nm). d) Photocurrent dynamics of graphene-Chla upon cycles of dark and light (200 ms each). Diagram of the energy level of e) n-doping effect graphene-Chla when the light is off and f) relative variation upon illumination. Reproduced with permission.[31] Copyright 2013, Elsevier Ltd.

the HOMO-LUMO transition. The hole carriers thus generated are energetically favorable to be transferred to graphene layer (p-type doping) as shown in Figure 12f, generating a supplementary electric field at Chl/graphene interface, opposite to the built-in one, further demonstrated by the photoluminescence light-quenching. Moreover, if the supplementary electric field is enhanced by higher excitation power, the screening effect at the interface becomes more important in the overall electric field, and therefore the carrier transfer is less efficient. The photocurrent action spectrum further underlines the active role of Chl in the device, showing also a red-shift compared to the Chl solution absorption spectra (Figure 12b) due to the supramolecular chlorin rings stacking, leading to a loss of excitation energy.[54] Photoinduced carrier concentration of about 10^{12} cm^{-2} under an irradiance of 100 mW cm^{-2} was detected. By applying V_{GS} –55V and an excitation power of 22 mW cm^{-2}, a positive photocurrent signal was detected, reverting to the base level in the dark (Figure 12d). Electron–hole mobility was found to increase by increasing excitation power. Carrier concentration was also found to increase with the thickness of the photoactive component, indicating that the carriers can diffuse within the film and then transfer to graphene layer. By increasing the

illumination power, even though more electron–hole pairs are generated, the responsivity tends to decrease,[55] because the charge transfer rate decreases reaching the saturation of the electrons trapping. Therefore, the maximum responsivity is obtained as the excitation power P approaches zero. The relevant responsivity for the proposed device was found about 10^6 A W^{-1}, with a quantum efficiency (QE) of about 0.008% for a 10 pW illumination power, resulting from the synergic contribution of Chls photoresponse and graphene high charge carrier mobility. The overall device performance was found better compared to other graphene-based systems using quantum dots[56] and C_{60}[57] as sensitizers.

Another interesting Chls-based phototransistor was developed more recently by Lin et al.,[58] focusing their work on the fabrication of transient device technology, that is, a device that after fulfilling its function can physically disappear as a response of an external stimulus.[59] Such devices raise both industrial and academic interest,[60] finding application from biomedical (e.g., targeted drug delivery matrices, injectable sensors, or temporary digital-imaging devices) to military field (e.g., sensors, cameras, antennas, and other spy gears),[61] reducing environmental wastes.

The proposed device consists of a dissolvable, eco compatible, and flexible photodetector similar to the one proposed by Chen et. al.,[31] with a combination of graphene and Chl-*a*, used also this case as sensitizer. Chl biodegradability and biocompatibility make it perfectly suitable as active material in transient devices. Instead of the most common Au, insoluble in a biocompatible matrix, the water soluble and biocompatible Mg was used as the electrode material.[61a,62] The device hence consisted of a gate of silicon/silicon dioxide drop-coated with poly(vinyl alcohol) (PVA), in turn coated with p-type CVD-graphene. The Mg electrodes were patterned onto the graphene and finally the Chl layer was deposited by spin-coating.

Upon water exposure, the device starts to decompose (**Figure 13**a–c) beginning from the PVA (6 min) and finally the electrode (30 min), demonstrating the transient feature of the system, while the remaining graphene thin atomic layer is not of any substantial environmental concern.

The electronic performance was screened by *I*–*V* and photoresponse (current over time) study, using a 656 nm laser. Upon illumination, as already described, electron–hole couples are generated within the Chl layer and, due to the energy levels alignment, a further hole doping of the p-graphene occurs, enhancing the current output. By decreasing the excitation power, both photocurrent and response time decrease (Figure 13d). The first effect is due to the decrease of charge generation at the head of the photoinduced process, while the second could be related to increase of charges trapped in the interface defects between the layers. Moreover, when the laser is turned off, the free charge carriers recombine very fast while the bounded charges need more time for complete the recombination, resulting in a biexponential decay.[63] The I_{DS}–V_{GS} graph in Figure 13e shows that the Dirac point shifts in a way characteristic of the modification in the graphene structure.[59c] With the only graphene layer, the Dirac point is at +19.5 V, then, after deposition of the Chl layer, shifts at +6 V in dark condition and +13 V under 1.7 μW laser illumination, similarly to what found by Chen et al.[31] Maximum photocurrent gain of 600 and maximum device responsivity of about 200 AW^{-1} were recorded with V_{DS} = 1 V and 50 μW power light. The significantly lower photoresponsivity compared to the value of ≈10^6 AW^{-1} obtained by Chen et al.[31] is possibly due to their higher graphene and substrate quality, assembled with a resist-free technique to preserve the high charge carrier mobility of the graphene. The lower performance is however also a consequence of the dissolvable and flexible nature of the device, since for example, the Mg electrodes induce defects in the graphene structure generating a resistive junction. The device was tested under different bending curvature radius, without substantial differences in performances, mainly related to the reduced incident radiation density rather than to the device efficiency itself.

3.5. Devices Based on Chlorosome-Like Structures

As already mentioned, BChl-*c* is able to form extraordinary scaffold-free self-organized J-type aggregates found in chlorosomes of Green Bacteria thanks to the absence of the bulky 13^2-$COOCH_3$ substituent in its chlorin ring and the presence of an −OH group in $C3^1$. With respect to monomeric BChl-*c*, which exhibit the adsorption bands at 660/670 and 432/445 nm (typical of chlorin-based pigments), self-assembled BChl-*c* molecules exhibit a large red-shift of the absorption bands, due to strong excitonic coupling among the pigments.[64] Simplified versions of chlorosome structures, through self-assembly of native[17] or semisynthetic chlorophylls[65] can be easily prepared in vitro with the so-called dilution assembly method[66] by diluting a concentrated solution of monomeric BChl-c with appropriate solvents (e.g., cyclohexane, water, hexane, etc.) at controlled temperature and concentration. Artificial BChl-*c* J-aggregates represent new bio-inspired materials suitable for solar cells and artificial photosynthesis, due to their facile preparation, protein-free scaffold structure, and for their peculiar spectroscopic features.

A chlorosome-inspired artificial light harvesting model has been proposed in a simple photodevice mimicking the energy transfer pathway of Green Bacteria.[67] BChl-*c* aggregates have been entrapped in a vesicle made of a block copolymer (**Figure 14**a,b), leading to a biohybrid light harvesting ellipsoid nanocomposite featuring a red shifted Q_Y absorption band to 730 nm. Semi-physiologic function was further demonstrated by successful EET, with 55% efficiency, to an external membrane-bound energy acceptor (DiR dye) intercalated into a bilayer film (Figure 14c,d). The process well resembled all the EET system of chlorosomes, paving the way for the assembly of stable artificial photosynthetic systems.

However, rather than the natural BChl-*c*, semisynthetic Zn of H derivatives are more often used for optoelectronic applications, all sharing the characteristic of lacking the 13^2-$COOCH_3$ substituent, thereby forming J-aggregates of various shapes, leading to high semiconducting charge carrier mobilities. For instance, mobilities of 0.07 cm^2 V^{-1} s^{-1} for tubular assemblies of 3^1-hydroxy ZnChls and up to 0.28 cm^2 V^{-1} $s^{-1}$for 2D stacked assemblies of 3^1-methoxy ZnChls (**Figure 15**a) were found in the solid state by pulsed radiolysis time-resolved microwave conductivity measurement,[37] even though this technique usually yields larger mobility values than OFET measurements.

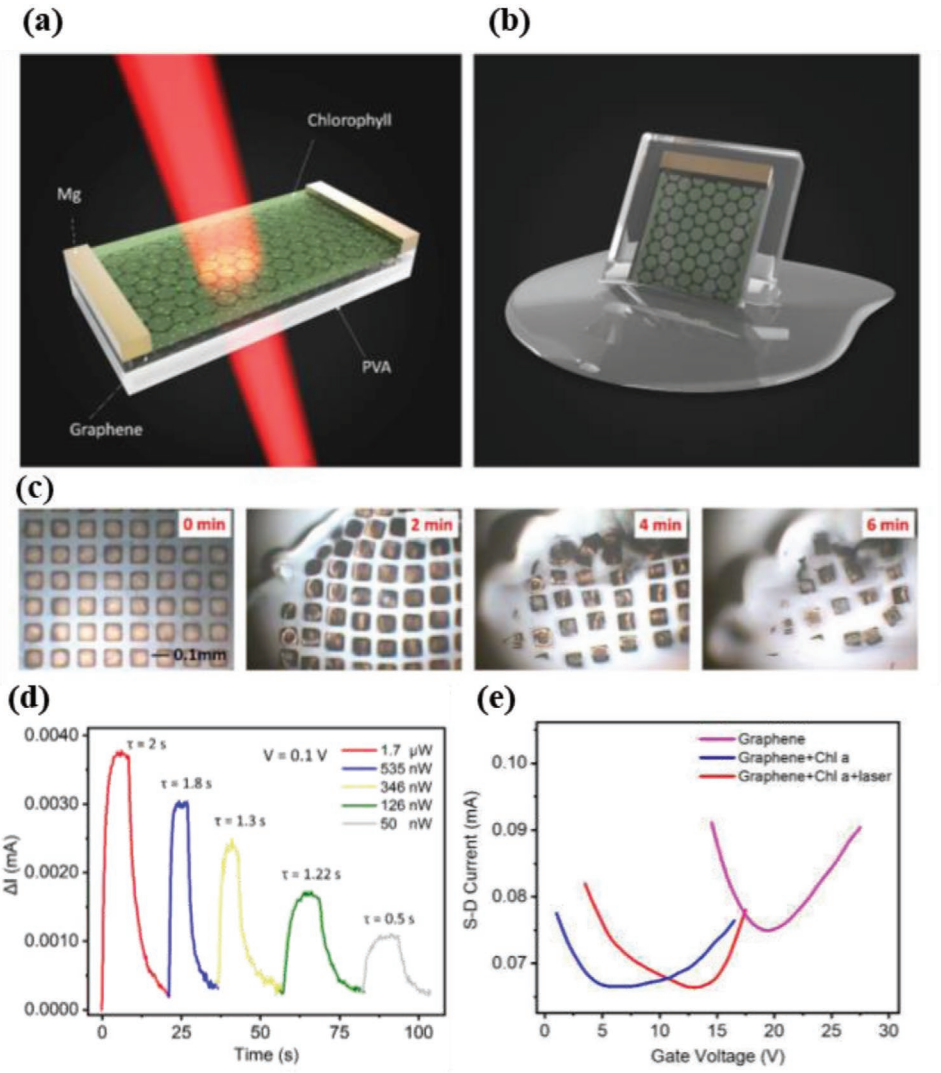

Figure 13. a,b) Schematic representation of the transient photodetector before and during dissolving process. c) Timeline of the dissolving process of the photodetector device, showing the first dissolution of PVA substrate that starts at 2 min. d) Photocurrent response over time under different excitation power. e) Dirac point shift comparing pristine graphene and the modified one, both in a dark state and under illumination. Reproduced with permission.[58] Copyright 2018, American Chemical Society.

On this ground, the biosolar cell shown in Figure 15b has been proposed to exploit different semisynthetic Chl derivatives acting as a hole transporters in form of organized aggregates and as sensitizers bound to TiO_2 nanoparticles.[67b] BSC are devices closely mimicking the photosynthesis process since they use only photosynthetic pigments as photoactive materials to perform the two tasks of radiant energy capturing and charge separation/transport. The key point is the different spatial organization of the pigments (ordered large aggregates for charge transport and monomers/small aggregates for light capturing and electron injection into the TiO_2) communicating through a heterojunction. In details, the BChl-c derivatives, shown in Figure 15b, were a) ZnChl-1, featuring a hydroxymethyl group at the C3 position, capable of forming coordinating HO/Zn bond with adjacent molecules generating J-aggregates with high charge mobility and b) H_2Chl-2 bearing a carboxy group at the C3[2] position for covalent bonding with the TiO_2 nanocrystalline films. The absorption spectrum of ZnChl-1 broadens passing from THF solution to the solid state (spin-coated on TiO_2), indicating the formation of J-aggregates. The carrier mobility of ZnChl-1 thin film was determined in an OFET device. Highly doped n-type Si was used as the gate, with a thermally grown 300-nm SiO_2 layer serving as the gate dielectric. ZnChl-1 film with a 100-nm thickness was prepared by spin coating from a THF solution, obtaining an aggregation similar to that on TiO_2. Gold source and drain electrodes were deposited using shadow mask on top of the semiconductor film. ZnChl-1 resulted to be a p-type semiconductor, as found for Chl-a spin-coated thin film,[42] with carrier mobility of 6.2×10^{-4} cm^2 V^{-1} s^{-1}. The device featured ON/OFF ratio of 3.5×10^3, and threshold voltage of –7.1 V. As expected, the carrier mobility is substantially smaller than the perfectly aligned ZnChl-1 aggregates,[37] but is comparable with other hole transporters such as poly(3-hexylthiophene) (P3HT). The LUMO of

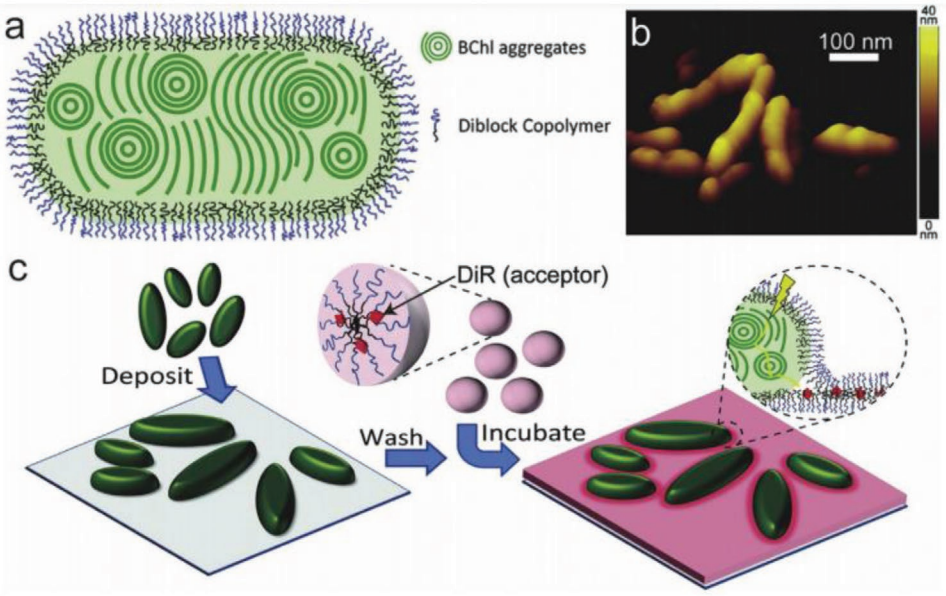

Figure 14. a) Scheme of a biohybrid nanocomposite composed of block copolymers and self-aggregates of natural BChl-c. b) AFM image of these nanocomposites in 3D reconstruction; c) scheme of an artificial EET system mimicked a chlorosome with baseplate proteins. Adapted with permission.[67a] Copyright 2018, Royal Society of Chemistry.

H_2Chl-2 is sufficiently above the CB of TiO_2, so that the photoexcited electrons are transferred to TiO_2. Moreover, ZnChl-1 HOMO is above that of H_2Chl-2, resulting in an effective hole transfer from the cation radicals of H_2Chl-2 to ZnChl-1. The solar cell exhibited relatively modest performance with power conversion efficiency (PCE) of around 0.11%, possibly due to poor the hole transfer between ZnChl-1 and the cation radical of H_2Chl-2 compared to electrolyte-based solar cells. Improved performances were obtained using the Chl derivative of ref. [37] forming the tubular aggregates shown in Figure 15a. Its spin-coated thin film showed charge carrier mobility of 4.11×10^{-3} cm^2 V^{-1} s^{-1} due to the better ordered structure of J-type aggregates. The resulting device showed a PCE of around 0.89%,[68] that was further improved to 2.1% controlling the film surface roughness by optimizing the solvents used for the deposition.[69] Therefore, semisynthetic Chl derivatives able to form aggregates similar to those formed by BChl-c in chlorosomes as hole transporting material coupled with Chls derivatives able to bind to TiO_2 for electron injection are promising materials for producing totally biocompatible sensitized thin-film solar cells.

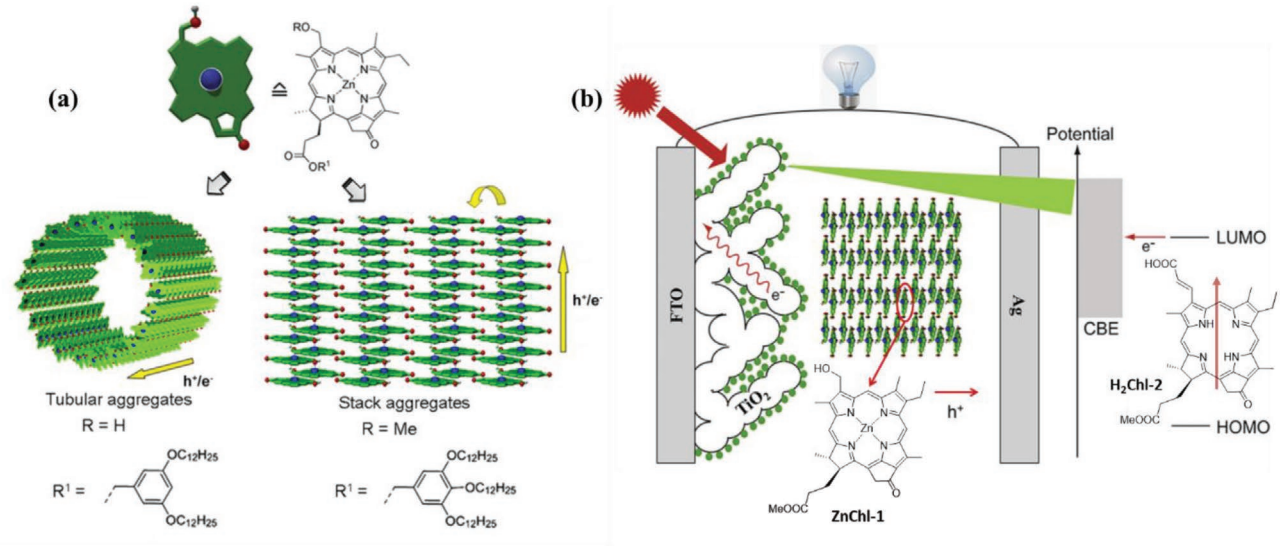

Figure 15. a) Chemical structures and self-assembled architectures of semisynthetic 3^1-hydroxy and 3^1-methoxy zinc chlorins. Adapted with permission.[37] Copyright 2012, American Chemical Society. b) Biosolar cell using two different Chl derivatives, one forming J-aggregates for hole transport and one covalently bound to TiO_2 for photoexcited electron injection. Adapted with permission.[67b] Copyright 2015, Elsevier.

4. Conclusion

In this review we have summarized the structural and physicochemical characteristics of (B)Chls, the most abundant natural pigment involved in photosynthesis, and surveyed the recent literature about their use in bio-hybrid optoelectronics devices, with special focus on their semiconducting capability. After a brief overview of the biosynthetic pathway of (B)Chls, which can be an important guide in selection and design of Chls-based semiconductors, we have described their spectroscopic properties and their role as active species in optoelectronics. Their highly conjugated core macrocycles (porphyrin, chlorin or bacteriochlorin type) (B)Chls make them organic molecular semiconductors in the solid state, with charge carrier mobility comparable to that of other organic synthetic counterparts. The use of (B)Chls in optoelectronic devices combines the advantages of synthetic organic semiconductors (low cost, room temperature processing, compatibility with plastic substrates, and chemical tunability) with their massive abundance in natural, nontoxicity, and biodegradability. Moreover (B)Chls feature extremely large extinction coefficients in the blue and red to far red regions, making them suitable for the construction of light-activated devices. Different architectures of OFETs have been proposed and characterized, both with (B)Chl as the sole bio-organic species or used as sensitizer for another organic semiconductor to endow it with light sensitivity. Finally, inspired by the J-aggregates of BChl-c found in chlorosomes, biosolar cells entirely relying on semisynthetic Chl derivatives have been proposed, providing new perspectives on using bio-resources for electricity production but also contributing to unveil the opto-electrical and physicochemical properties that should be optimized for effective biosupramolecular materials integration in hybrid devices. As an interesting perspective, (B)Chls could be exploited as OSC in electrolyte-gated field effect transistors (EGOFET). This relatively new FET architecture, first demonstrated in 2010 by Kergoat and coworkers,[70] offers potentially several advantages with respect to the traditional FETs, still linked to conventional dielectrics like SiO_2, with low dielectric constants (up to hundreds of nF) limiting their application as low power devices. On the opposite, in EGOFET aqueous electrolyte solutions where an electrical double layer (EDL) forming at the electrolyte/OSC interface can effectively serve as dielectric. The EDL thickness of tens of Å and capacitance on the order of 1–10 μF cm^{-2} enables operation at significantly reduced voltages (<2 V).[71] Moreover, the use of aqueous electrolytes is of great interest for applications in the field of bioelectronics and biosensing.[72] Typical OSC used for EGOFETs include polymers like poly(3-hexylthiophene-2,5-diyl) (P3HT)[70] and poly[2,5-bis(3-tetradecylthiophen-2-yl)thieno[3,2-b]thiophene] (pBTTT)[73] or molecules like rubene[70] and Cu(II) phthalocyanine (CuPc).[74] (B)Chls are naturally stable in aqueous media and should retain high carrier mobility, especially in the form of J-aggregates. Moreover, their high absorption cross section could endow EGOFET of interesting photoresponsivity.

Acknowledgements

Funded by the European Union's Horizon 2020 Research and Innovation Programme under grant agreement No. 800926 (HyPhOE, Hybrid Electronics Based on Photosynthetic Organisms).

Conflict of Interest

The authors declare no conflict of interest.

Keywords

bio-optoelectronic, chlorophylls, organic semiconductor, photonics, phototransistors, supramolecular aggregates

Received: February 28, 2021
Revised: April 15, 2021
Published online:

[1] a) R. E. Blankenship, H. Hartman, *Trends Biochem. Sci.* **1998**, *23*, 94; b) H. Hartman, *Origins Life Evol. Biospheres* **1998**, *28*, 515; c) J. Raymond, D. Segrè, *Science* **2006**, *311*, 1764; d) M. F. Hohmann-Marriott, R. E. Blankenship, *Annu. Rev. Plant Biol.* **2011**, *62*, 515.
[2] a) D. F. Ghanotakis, G. Tsiotis, T. M. Bricker, in *Concepts in Photobiology: Photosynthesis and Photomorphogenesis* (Eds: G. S. Singhal, G. Renger, S. K. Sopory, K. D. Irrgang, Govindjee), Springer Netherlands, Dordrecht **1999**, p. 264; b) P. Manna, P. R. Chitnis, in *Concepts in Photobiology: Photosynthesis and Photomorphogenesis* (Eds: G. S. Singhal, G. Renger, S. K. Sopory, K. D. Irrgang, Govindjee), Springer Netherlands, Dordrecht **1999**, p. 221.
[3] a) M. P. Johnson, *Essays Biochem.* **2016**, *60*, 255; b) T. Cardona, *Photosynth. Res.* **2015**, *126*, 111; c) R. S. Gupta, B. Khadka, *Photosynth. Res.* **2016**, *127*, 201.
[4] a) A. G. M. Chew, D. A. Bryant, *Annu. Rev. Microbiol.* **2007**, *61*, 113; b) K. Vogl, M. Tank, G. Orf, R. Blankenship, D. Bryant, *Front. Microbiol.* **2012**, *3*, 298.
[5] a) K. Hajdu, T. Szabó, A. E. Sarrai, L. Rinyu, L. Nagy, *Int. J. Photoenergy* **2017**, *2017*, 9128291; b) F. Milano, A. Punzi, R. Ragni, M. Trotta, G. M. Farinola, *Adv. Funct. Mater.* **2019**, *29*, 1805521; c) J. Z. Zhang, E. Reisner, *Nat. Rev. Chem.* **2020**, *4*, 6.
[6] a) M. L.o Presti, M. M. Giangregorio, R. Ragni, L. Giotta, M. R. Guascito, R. Comparelli, E. Fanizza, R. R. Tangorra, A. Agostiano, M. Losurdo, G. M. Farinola, F. Milano, M. Trotta, *Adv. Electron. Mater.* **2020**, *6*, 2000140; b) S. K. Ravi, Z. Yu, D. J. K. Swainsbury, J. Ouyang, M. R. Jones, S. C. Tan, *Adv. Energy Mater.* **2017**, *7*, 1601821.
[7] N. Paul, L. Suresh, J. V. Vaghasiya, L. Yang, Y. Zhang, D. K. Nandakumar, M. R. Jones, S. C. Tan, *Biosens. Bioelectron.* **2020**, *165*, 112423.
[8] A. H. Teodor, B. D. Bruce, *Trends Biotechnol.* **2020**, *38*, 1329.
[9] a) M. Di Lauro, S. la Gatta, C. A. Bortolotti, V. Beni, V. Parkula, S. Drakopoulou, M. Giordani, M. Berto, F. Milano, T. Cramer, M. Murgia, A. Agostiano, G. M. Farinola, M. Trotta, F. Biscarini, *Adv. Electron. Mater.* **2019**, *6*, 1900888; b) A. Takshi, H. Yaghoubi, D. Jun, J. T. Beatty, *Electronics* **2020**, *9*, 1709.
[10] a) S. K. Ravi, N. Paul, L. Suresh, A. T. Salim, T. Wu, Z. Wu, M. R. Jones, S. C. Tan, *Mater. Horiz.* **2020**, *7*, 866; b) S. K. Ravi, T. Wu, V. S. Udayagiri, X. M. Vu, Y. Wang, M. R. Jones, S. C. Tan, *Adv. Mater.* **2018**, *30*, 1802290.
[11] a) E. D. Glowacki, R. R. Tangorra, H. Coskun, D. Farka, A. Operamolla, Y. Kanbur, F. Milano, L. Giotta, G. M. Farinola, N. S. Sariciftci, *J. Mater. Chem. C* **2015**, *3*, 6554; b) D. Nishiori, W. Zhu, R. Salles, M. Miyachi, Y. Yamanoi, T. Ikuta, K. Maehashi, T. Tomo, H. Nishihara, *ACS Appl. Mater. Interfaces* **2019**, *11*, 42773.
[12] S. K. Ravi, V. S. Udayagiri, L. Suresh, S. C. Tan, *Adv. Funct. Mater.* **2017**, *28*, 1705305.
[13] G. P. MOSS, *Eur. J. Biochem.* **1988**, *178*, 277.
[14] G. Layer, J. Reichelt, D. Jahn, D. W. Heinz, *Protein Sci.* **2010**, *19*, 1137.

[15] D. P. Bednarik, J. K. Hoober, *Arch. Biochem. Biophys.* **1985**, *240*, 369.
[16] N. Wakao, N. Yokoi, N. Isoyama, A. Hiraishi, K. Shimada, M. Kobayashi, H. Kise, M. Iwaki, S. Itoh, S. Takaichi, *Plant Cell Physiol.* **1996**, *37*, 889.
[17] T. Miyatake, H. Tamiaki, *J. Photochem. Photobiol., C* **2005**, *6*, 89.
[18] H. Scheer, in *Chlorophylls and Bacteriochlorophylls: Biochemistry, Biophysics, Functions and Applications* (Eds: B. Grimm, R. J. Porra, W. Rüdiger, H. Scheer), Springer Netherlands, Dordrecht **2006**, p. 1.
[19] R. Croce, H. van Amerongen, *Nat. Chem. Biol.* **2014**, *10*, 492.
[20] D. Noy, R. Yerushalmi, V. Brumfeld, I. Ashur, H. Scheer, K. K. Baldridge, A. Scherz, *J. Am. Chem. Soc.* **2000**, *122*, 3937.
[21] R. E. Blankenship, in *Molecular Mechanisms of Photosynthesis* (Ed: R. E. Blankenship), Wiley Blackwell, Hoboken, NJ **2002**, p. 42.
[22] a) R. E. Blankenship, in *Molecular Mechanisms of Photosynthesis* (Ed: R. E. Blankenship), Wiley Blackwell, Hoboken, NJ **2002**, p. 61; b) R. E. Blankenship, in *Molecular Mechanisms of Photosynthesis* (Ed: R. E. Blankenship), Wiley Blackwell, Hoboken, NJ **2002**, p. 124; c) S. Bahatyrova, R. N. Frese, C. A. Siebert, J. D. Olsen, K. O. van der Werf, R. van Grondelle, R. A. Niederman, P. A. Bullough, C. Otto, C. N. Hunter, *Nature* **2004**, *430*, 1058.
[23] J. Alster, M. Kabeláč, R. Tuma, J. Pšenčík, J. V. Burda, *Comput. Theor. Chem.* **2012**, *998*, 87.
[24] S. Matsubara, H. Tamiaki, *J. Photochem. Photobiol., C* **2020**, *45*, 100385.
[25] M. Li, Y. Li, S.-i. Sasaki, J. Song, C. Wang, H. Tamiaki, W. Tian, G. Chen, T. Miyasaka, X.-F. Wang, *ChemSusChem* **2016**, *9*, 2862.
[26] W. Zhao, C. Dall'Agnese, S. Duan, Y. Sanehira, Y. Wei, H. Tamiaki, S.-i. Sasaki, X.-F. Wang, *ACS Energy Lett.* **2019**, *4*, 384.
[27] Y. Li, X. Chen, Y. Sun, X. Meng, Y. Dall'Agnese, G. Chen, C. Dall'Agnese, H. Ren, S.-i. Sasaki, H. Tamiaki, X.-F. Wang, *Adv. Mater. Interfaces* **2020**, *7*, 1902080.
[28] R. Mandal, G. Dutta, *Sens. Int.* **2020**, *1*, 100058.
[29] S. Duan, Q. Zhou, A. Li, X.-F. Wang, S.-i. Sasaki, H. Tamiaki, *Sol. RRL* **2020**, *4*, 2000162.
[30] A. Mahmood, J.-Y. Hu, B. Xiao, A. Tang, X. Wang, E. Zhou, *J. Mater. Chem. A* **2018**, *6*, 16769.
[31] S.-Y. Chen, Y.-Y. Lu, F.-Y. Shih, P.-H. Ho, Y.-F. Chen, C.-W. Chen, Y.-T. Chen, W.-H. Wang, *Carbon* **2013**, *63*, 23.
[32] M. Oehzelt, N. Koch, G. Heimel, *Nat. Commun.* **2014**, *5*, 4174.
[33] F. Garnier, *Curr. Opin. Solid State Mater. Sci.* **1997**, *2*, 455.
[34] M. Takada, H. Yoshioka, H. Tada, K. Matsushige, *Jpn. J. Appl. Phys.* **2002**, *41*, L73.
[35] G. Horowitz, F. Kouki, P. Spearman, D. Fichou, C. Nogues, X. Pan, F. Garnier, *Adv. Mater.* **1996**, *8*, 242.
[36] H. Dong, X. Fu, J. Liu, Z. Wang, W. Hu, *Adv. Mater.* **2013**, *25*, 6158.
[37] S. Patwardhan, S. Sengupta, L. D. A. Siebbeles, F. Würthner, F. C. Grozema, *J. Am. Chem. Soc.* **2012**, *134*, 16147.
[38] H. Bässler, A. Köhler, in *Unimolecular and Supramolecular Electronics I. Topics in Current Chemistry* (Ed: R. Metzger), Springer, Berlin **2011**, p. 321.
[39] R. T. Tung, *Appl. Phys. Rev.* **2014**, *1*, 011304.
[40] A. Terenin, E. Putzeiko, I. Akimov, *Discuss. Faraday Soc.* **1959**, *27*, 83.
[41] C. W. Tang, A. C. Albrecht, *J. Chem. Phys.* **1975**, *62*, 2139.
[42] Y. Yu, Y. Zhang, L. Jin, Z. Chen, Y. Li, Q. Li, M. Cao, Y. Che, H. Dai, J. Yang, J. Yao, *Org. Electron.* **2019**, *65*, 381.
[43] G. Konstantatos, M. Badioli, L. Gaudreau, J. Osmond, M. Bernechea, F. P. G. de Arquer, F. Gatti, F. H. L. Koppens, *Nat. Nanotechnol.* **2012**, *7*, 363.
[44] a) W. M. Campbell, A. K. Burrell, D. L. Officer, K. W. Jolley, *Coord. Chem. Rev.* **2004**, *248*, 1363; b) H. Spanggaard, F. C. Krebs, *Sol. Energy Mater. Sol. Cells* **2004**, *83*, 125.
[45] D. S. Hecht, R. J. A. Ramirez, M. Briman, E. Artukovic, K. S. Chichak, J. F. Stoddart, G. Grüner, *Nano Lett.* **2006**, *6*, 2031.
[46] Z. Sun, Z. Liu, J. Li, G.-a. Tai, S.-P. Lau, F. Yan, *Adv. Mater.* **2012**, *24*, 5878.
[47] S. Lee, A. Tang, S. Aloni, H. S. Philip Wong, *Nano Lett.* **2016**, *16*, 276.
[48] Y. Zhang, T.-T. Tang, C. Girit, Z. Hao, M. C. Martin, A. Zettl, M. F. Crommie, Y. R. Shen, F. Wang, *Nature* **2009**, *459*, 820.
[49] a) R. R. Nair, P. Blake, A. N. Grigorenko, K. S. Novoselov, T. J. Booth, T. Stauber, N. M. R. Peres, A. K. Geim, *Science* **2008**, *320*, 1308; b) C. Casiraghi, A. Hartschuh, E. Lidorikis, H. Qian, H. Harutyunyan, T. Gokus, K. S. Novoselov, A. C. Ferrari, *Nano Lett.* **2007**, *7*, 2711.
[50] a) E. J. H. Lee, K. Balasubramanian, R. T. Weitz, M. Burghard, K. Kern, *Nat. Nanotechnol.* **2008**, *3*, 486; b) T. Mueller, F. Xia, M. Freitag, J. Tsang, P. Avouris, *Phys. Rev. B* **2009**, *79*, 245430; c) X. Xu, N. M. Gabor, J. S. Alden, A. M. van der Zande, P. L. McEuen, *Nano Lett.* **2010**, *10*, 562; d) M. Freitag, T. Low, F. Xia, P. Avouris, *Nat. Photonics* **2013**, *7*, 53.
[51] a) F. Bonaccorso, Z. Sun, T. Hasan, A. C. Ferrari, *Nat. Photonics* **2010**, *4*, 611; b) Q. Bao, K. P. Loh, *ACS Nano* **2012**, *6*, 3677; c) P. Avouris, F. Xia, *MRS Bull.* **2012**, *37*, 1225.
[52] a) Y.-J. Yu, Y. Zhao, S. Ryu, L. E. Brus, K. S. Kim, P. Kim, *Nano Lett.* **2009**, *9*, 3430; b) C. Oshima, A. Nagashima, *J. Phys.: Condens. Matter* **1997**, *9*, 1.
[53] a) H. Ishii, K. Seki, *IEEE Trans. Electron Devices* **1997**, *44*, 1295; b) I. G. Hill, A. Rajagopal, A. Kahn, Y. Hu, *Appl. Phys. Lett.* **1998**, *73*, 662.
[54] H. Heithiert, K. Ballschmiter, H. Mohwald, *Photochem. Photobiol.* **1983**, *37*, 201.
[55] a) W. Guo, S. Xu, Z. Wu, N. Wang, M. M. T. Loy, S. Du, *Small* **2013**, *9*, 3031; b) C. Soci, A. Zhang, B. Xiang, S. A. Dayeh, D. P. R. Aplin, J. Park, X. Y. Bao, Y. H. Lo, D. Wang, *Nano Lett.* **2007**, *7*, 1003.
[56] D. Zhang, L. Gan, Y. Cao, Q. Wang, L. Qi, X. Guo, *Adv. Mater.* **2012**, *24*, 2715.
[57] E.-K. Jeon, C.-S. Yang, Y. Shen, T. Nakanishi, D.-s. Jeong, J.-J. Kim, K.-s. Ahn, K.-j. Kong, J.-O. Lee, *Nanotechnology* **2012**, *23*, 455202.
[58] S.-Y. Lin, G. Haider, Y.-M. Liao, C.-H. Chang, W.-J. Lin, C.-Y. Su, Y.-R. Liou, Y.-F. Huang, H.-I. Lin, T.-C. Chung, T.-Y. Lin, Y.-F. Chen, *ACS Appl. Nano Mater.* **2018**, *1*, 5092.
[59] a) K. K. Fu, Z. Wang, J. Dai, M. Carter, L. Hu, *Chem. Mater.* **2016**, *28*, 3527; b) Y. Gao, Y. Zhang, X. Wang, K. Sim, J. Liu, J. Chen, X. Feng, H. Xu, C. Yu, *Sci. Adv.* **2017**, *3*, e1701222; c) X. Shi, Y.-M. Liao, H.-Y. Lin, P.-W. Tsao, M.-J. Wu, S.-Y. Lin, H.-H. Hu, Z. Wang, T.-Y. Lin, Y.-C. Lai, Y.-F. Chen, *ACS Nano* **2017**, *11*, 7600; d) S.-W. Hwang, C. H. Lee, H. Cheng, J.-W. Jeong, S.-K. Kang, J.-H. Kim, J. Shin, J. Yang, Z. Liu, G. A. Ameer, Y. Huang, J. A. Rogers, *Nano Lett.* **2015**, *15*, 2801.
[60] H. Acar, S. Çınar, M. Thunga, M. R. Kessler, N. Hashemi, R. Montazami, *Adv. Funct. Mater.* **2014**, *24*, 4135.
[61] a) S.-W. Hwang, H. Tao, D.-H. Kim, H. Cheng, J.-K. Song, E. Rill, M. A. Brenckle, B. Panilaitis, S. M. Won, Y.-S. Kim, Y. M. Song, K. J. Yu, A. Ameen, R. Li, Y. Su, M. Yang, D. L. Kaplan, M. R. Zakin, M. J. Slepian, Y. Huang, F. G. Omenetto, J. A. Rogers, *Science* **2012**, *337*, 1640; b) S.-W. Hwang, D.-H. Kim, H. Tao, T.-i. Kim, S. Kim, K. J. Yu, B. Panilaitis, J.-W. Jeong, J.-K. Song, F. G. Omenetto, J. A. Rogers, *Adv. Funct. Mater.* **2013**, *23*, 4087; c) G. Gollavelli, Y.-C. Ling, *Biomaterials* **2012**, *33*, 2532.
[62] a) S. Keim, J. G. Brunner, B. Fabry, S. Virtanen, *J. Biomed. Mater. Res., Part B* **2011**, *96B*, 84; b) L. Yin, H. Cheng, S. Mao, R. Haasch, Y. Liu, X. Xie, S.-W. Hwang, H. Jain, S.-K. Kang, Y. Su, R. Li, Y. Huang, J. A. Rogers, *Adv. Funct. Mater.* **2014**, *24*, 645.
[63] G. Haider, P. Roy, C.-W. Chiang, W.-C. Tan, Y.-R. Liou, H.-T. Chang, C.-T. Liang, W.-H. Shih, Y.-F. Chen, *Adv. Funct. Mater.* **2016**, *26*, 620.
[64] J. M. Olson, J. P. Pedersen, *Photosynth. Res.* **1990**, *25*, 25.
[65] a) A. Löhner, T. Kunsel, M. I. S. Röhr, T. L. C. Jansen, S. Sengupta, F. Würthner, J. Knoester, J. Köhler, *J. Phys. Chem. Lett.* **2019**, *10*, 2715; b) S. Ogi, C. Grzeszkiewicz, F. Würthner, *Chem. Sci.* **2018**, *9*, 2768.

[66] S. Shoji, T. Ogawa, T. Hashishin, H. Tamiaki, *ChemPhysChem* **2018**, *19*, 913.
[67] a) A. M. Collins, J. A. Timlin, S. M. Anthony, G. A. Montaño, *Nanoscale* **2016**, *8*, 15056; b) Y. Li, S.-i. Sasaki, H. Tamiaki, C.-L. Liu, J. Song, W. Tian, E. Zheng, Y. Wei, G. Chen, X. Fu, X.-F. Wang, *J. Power Sources* **2015**, *297*, 519.
[68] Y. Li, W. Zhao, M. Li, G. Chen, X.-F. Wang, X. Fu, O. Kitao, H. Tamiaki, K. Sakai, T. Ikeuchi, S.-i. Sasaki, *Chem. - Eur. J.* **2017**, *23*, 10886.
[69] W. Zhao, S.-i. Sasaki, H. Tamiaki, Y. Sanehira, Y. Wei, G. Chen, X.-F. Wang, *Org. Electron.* **2018**, *59*, 419.
[70] L. Kergoat, L. Herlogsson, D. Braga, B. Piro, M.-C. Pham, X. Crispin, M. Berggren, G. Horowitz, *Adv. Mater.* **2010**, *22*, 2565.
[71] S. H. Kim, K. Hong, W. Xie, K. H. Lee, S. Zhang, T. P. Lodge, C. D. Frisbie, *Adv. Mater.* **2013**, *25*, 1822.
[72] D. Wang, V. Noël, B. Piro, *Electronics* **2016**, *5*, 9.
[73] M. Y. Mulla, P. Seshadri, L. Torsi, K. Manoli, A. Mallardi, N. Ditaranto, M. V. Santacroce, C. Di Franco, G. Scamarcio, M. Magliulo, *J. Mater. Chem. B* **2015**, *3*, 5049.
[74] R. F. de Oliveira, L. Merces, T. P. Vello, C. C. Bof Bufon, *Org. Electron.* **2016**, *31*, 217.

Gabriella Buscemi received her Master's Degree in Molecular System Chemistry at the University of Palermo in 2017 dealing with the development of nanostructured systems based on alumino-silicate clay mineral, with application in both catalysis and drug-delivery systems. Currently she is working at the University of Bari as Ph.D. student in Chemical and Molecular Sciences within the HyPhOE project. Her research focuses on the development of hybrid electronic systems based on photosynthetic organism. Particular interest is given to the optimizations of electrode interface with tunable conductive polymers to enhance energy extraction, using as photoactive components photosynthetic bacteria, proteins, and algae.

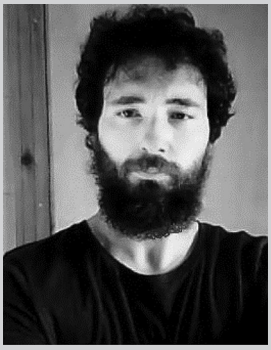

Danilo Vona is a researcher in Organic Chemistry at the Chemistry Department of the University of Bari "Aldo Moro," Italy. He is in charge of the project "Algambiente" (POR Puglia REFIN—Research for Innovation), regarding bioremediation of marine ecosystem. He specialized in interfacing biological components with inorganic and organic functional materials, in the frame of the European project on HyPhOE (Hybrid Electronics Based on Photosynthetic Organisms). During his Ph.D. in Organic Chemistry he worked on biohybrid systems based on biosilica extracted from diatoms microalgae. He has a degree in Medical and Pharmaceutical Biotechnology.

Massimo Trotta graduated in Chemistry in Bari in 1988. As an early-stage researcher, he spent two years at the Department of Biology at the University of Bologna and two years at the Department of Physics at the University of California in San Diego. He is officer of the Executive Committee of the European Society for Photobiology. Since 2005 he has been involved in the public understanding of science for nonspecialized audiences. His research topic is bacterial photosynthesis and environmental applications of the bacterial reaction center. He is working on soft polymers for improving electronic performances of photosynthetic bacteria.

Francesco Milano graduated in Chemistry in 1997 and received his Ph.D. in Chemical Sciences in 2001. He is a researcher at the Italian National Research Council. His research interests are in the investigation on bioelectronic applications involving bacterial photosynthesis, with a special focus on the functioning of the reaction center both for basic science and for applications like energy conversion and biosensing. He is actually working on soft polymers and liposomes preparation as membrane mimicking, for improving electronic-performances, and in drug delivery field.

Gianluca M. Farinola received his Ph.D. degree in Chemical Sciences in 1997 and is a full professor of Organic Chemistry at the University of Bari. He is adjunct professor in the Department of Biomedical Engineering of Tufts University. Gianluca is presently serving as the President of the EuChemS Division of Organic Chemistry. He is enrolled as a partner of the European HyPhOE project for the development of self-assembling conductive polymers for applications in bioelectronics. His research focuses on methods for photo/electro active organic materials and on the use of molecules, biopolymers, and nanostructures from living organisms in optoelectronic devices.